Available online at www.sciencedirect.com

ScienceDirect

Procedia Engineering 197 (2017) 3 – 12

Procedia Engineering

www.elsevier.com/locate/procedia

DYMAT 23rd Technical Meeting

Dynamic Fracture of Ductile Materials

Use of damage-based mesh adaptivity to predict ductile failure in blast-loaded aluminium plates

V.Aune[a,b,*], G. Valsamos[c], F. Casadei[c,1], M. Larcher[c], M. Langseth[a,b], T. Børvik[a,b]

[a] *Structural Impact Laboratory (SIMLab), Department of Structural Engineering, NTNU, Norwegian University of Science and Technology, NO-7491 Trondheim, Norway*

[b] *Centre for Advanced Structural Analysis (CASA), NTNU, NO-7491 Trondheim, Norway*

[c] *European Commission, Joint Research Centre (JRC), Directorate for Space, Security and Migration, Safety and Security of Buildings Unit, Via E. Fermi 2749, I-21027 Ispra (VA), Italy*

Abstract

This study uses experimental data to evaluate the capabilities of a numerical model in EUROPLEXUS (EPX) to predict ductile failure in thin aluminium plates subjected to blast loading. The loading was generated using a shock tube facility designed to expose structures to extreme loading conditions. The plates had an exposed area of 0.3 m × 0.3 m and experienced large deformations including failure at the supports at the largest blast intensities. Pressure measurements were synchronized with two high-speed cameras in a stereoscopic setup to capture the dynamic response using three-dimensional digital image correlation. The experimental results were used as basis for comparison to finite element (FE) simulations in EPX. Failure was introduced in the FE simulations using element erosion. Adaptive mesh refinement was applied in an attempt to describe the crack propagation observed in the experiments. The mesh refinement was driven by the damage parameter in the material model and occurred at user-defined levels. The numerical results were in good agreement with the experimental data, and were able to predict both the global deformation and the crack growth in the plates with good accuracy. The numerical model was also used to investigate the influence of FSI effects on the dynamic response of the plates. It was found that FSI may significantly mitigate the blast load acting on the plate, resulting in reduced deformations.

Peer-review under responsibility of the scientific committee of the International Conference on Dynamic Fracture of Ductile Materials

* Corresponding author. Tel.: +47-73-59-47-05; fax: +47-73-59-47-01.
E-mail address: vegard.aune@ntnu.no
[1] Retired

Peer-review under responsibility of the scientific committee of the International Conference on Dynamic Fracture of Ductile Materials
doi:10.1016/j.proeng.2017.08.076

Keywords: Blast loading; J2 plasticity theory; damage-based adaptivity; element erosion; fluid-structure interaction; EUROPLEXUS

1. Introduction

Advanced numerical techniques are often required for sufficient insight when designing protective structures in blast environments. However, before such methods can be used it is essential to evaluate their performance in terms of robustness, reliability and effectiveness in predicting both the loading and the dynamic response. Experimental validation is often preferred as it represents the actual physics in the problem, and controlled small-scale experiments could be used to evaluate current computational methods [1][2]. When considering ductile materials, these loading conditions may involve large inelastic strains, high strain rates, temperature softening and failure.

Plated structures are frequently used in blast-resistant design and these structures are typically made with geometries that closely resemble shell structures, where one of the dimensions (typically the thickness) is significantly smaller than the others. Such structures often require a fine mesh size to represent localization of damage and crack growth. This is due to the discrete nature of the finite element (FE) method which makes the failure mesh-sensitive since element erosion cannot occur in less than one element size. The mesh size will therefore influence both the localization of damage and the crack propagation, and it is necessary to use a sufficiently refined mesh in the vicinity of the crack. A refined mesh will also allow for element erosion without too much loss of mass in the plate. However, since the increase in CPU cost may be significant when uniformly refining the mesh, it is desirable to evaluate the capabilities of adaptive mesh refinement (AMR) in predicting ductile failure in blast-loaded plates. Recent advancements in the FE code EUROPLEXUS (EPX) [3] allow for AMR based on a user-defined threshold criterion, which make it convenient to relate the AMR to the damage evolution in the plate. AMR may also be of importance in other practical applications and in fluid-structure interaction (FSI) simulations, because a finer mesh is often needed in the fluid compared to that in the structure to obtain an accurate pressure field at the fluid-structure interface.

This motivated studies on the performance of damage-based AMR to predict failure of coarsely meshed shell structures exposed to blast loading. A series of shock tube experiments were therefore performed to establish a basis of comparison to the numerical simulations. The shock tube technique is favourable compared to airblast tests using high-explosives since it produces a controlled and repeatable blast loading in laboratory environments [4], and avoids the complexity of ground reflections, light flashes, fireballs and other potential challenges related to HE detonations. Piezoelectric pressure sensors were employed for pressure recordings, and these measurements were synchronized with two high-speed cameras in a stereoscopic setup to capture the dynamic response using three-dimensional digital image correlation (3D-DIC). Synchronization of the pressure measurements with the dynamic response enabled a thorough assessment of the dynamic failure process and of potential FSI effects.

The numerical simulations of the blast-loaded plates were performed in the explicit FE code EPX [3]. The objective of this study was (1) to look into the capabilities of damage-based AMR to predict ductile failure in blast-loaded plates and (2) to investigate the influence of FSI effects on the response of thin aluminium plates in blast environments. Material tests were also performed to determine the material behaviour at large plastic strains and to identify the parameter in an energy-based failure criterion.

2. Experimental work

2.1. Material tests

The 0.8-mm thick aluminium plates were manufactured from low-strength, strain-hardened and cold-rolled sheets of the alloy EN AW 1050-H14 produced by Hindalco Industries Ltd. This is 99.5 % pure aluminium subjected to annealing before being work hardened by rolling. The nominal yield stress and ultimate tensile strengths were given by the manufacturer to be 110 MPa and 116 MPa, respectively.

Tensile tests on dog-bone specimens from the base material were performed to determine the quasi-static behaviour of the material, while the dynamic material properties were taken from the literature [1][2]. The tests were performed in a Zwick/Roell Z030 testing machine at a constant deformation rate of 2.1 mm/min. This corresponds

to an initial strain rate of $\dot{\varepsilon} = 5 \times 10^{-4}$ s^{-1} for a gauge length of 70 mm. Three parallel tests were performed in three different directions ($0^{\circ}, 45^{\circ}, 90^{\circ}$) with respect to the rolling direction of the plate. Two-dimensional digital image

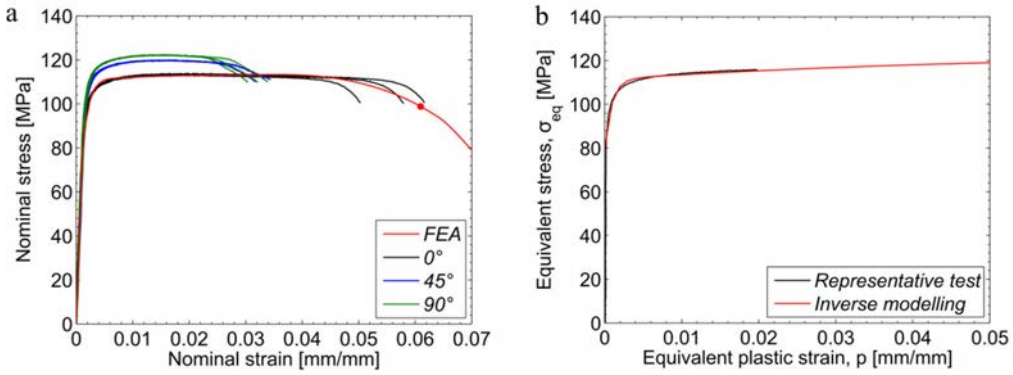

Figure 1. (a) Nominal stress-strain curves from uniaxial tension tests and simulation from EPX (FEA) with the material data from Table 2; (b) Equivalent stress-plastic strain curve until necking from a representative test in the rolling direction, and the extended Voce hardening rule based on the material parameters from the inverse modelling in Table 2.

correlation was used to measure the displacement field. These measurements were synchronized with the force measured by the hydraulic test machine at a sampling rate of 4 Hz.

The results are plotted as nominal stress-strain curves in Figure 1a, while Figure 1b presents the equivalent stress versus the plastic strain until necking from a representative test in the rolling direction. It is observed that the material is slightly anisotropic both in flow stress and elongation to failure.

2.2. Shock tube experiments

The blast tests were performed in the SIMLab Shock Tube Facility (SSTF) at NTNU. A detailed presentation of the design and evaluation of its performance can be found in Ref. [4]. This experimental technique is a well-defined

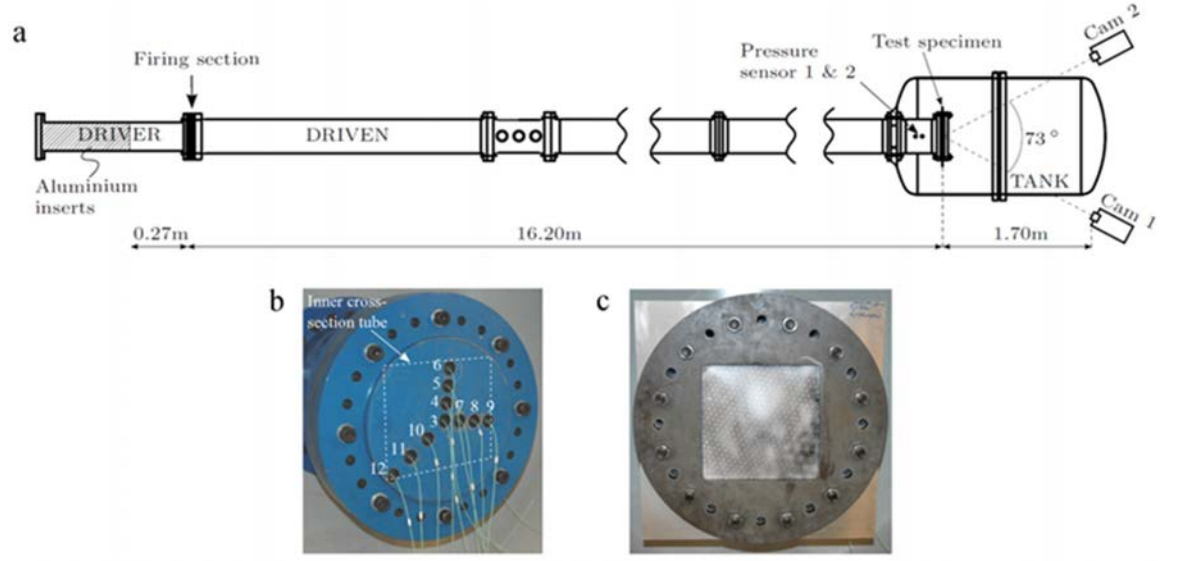

Figure 2. Experimental setup of the SIMLab Shock Tube Facility (SSTF): (a) Sketch of experimental setup (seen from above), picture of (b) massive steel plate and (c) clamping and DIC speckle pattern for the thin aluminium plate. Both the massive steel plate in (b) and the aluminium plate in (c) are seen from the cameras.

and easily controllable alternative to explosive detonations when generating blast loading, and consists of a gas-filled tube in which a high-pressure chamber (called driver in Figure 2a) is separated from a low-pressure chamber (denoted driven in Figure 2a) using multiple diaphragms. A sudden opening of the diaphragms generates a shock wave propagating downstream the diaphragms and into the low-pressure chamber, while rarefaction waves expand into the high-pressure chamber. Using a relatively small ratio between the lengths of the two pressure chambers, this experimental setup differs from traditional shock tubes in the way that the reflected rarefaction waves catch up with the shock wave resulting in pressure profiles similar to that from an explosive detonation. The properties of a planar blast wave acting on a structure may then be studied by placing a test specimen inside or at the end of the tube. A deformable test object will then enable the study of FSI effects during the dynamic response, where the pressure is affected by the structural response.

In the present work, the length of the driver and driven sections was 0.27 m and 16.20 m, respectively, both with a cross-sectional area of 0.09 m^2. The blast intensity was varied by changing the pressure in the driver section, while the pressure in the driven section was at ambient conditions. Table 1 gives the test matrix used herein, where each test is numbered XY in which X denotes rigid plate (R) or aluminium plate (A) and Y indicates the firing overpressure in bars in the driver. The massive plate was used to obtain a rigid blind flange (Figure 2b), while the thin aluminium plate was used to introduce moving boundary conditions (Figure 2c). Pressure measurements from the massive plate tests were used as a basis to investigate potential FSI effects in the tests with aluminium plates. Both the massive plate with thickness of 0.05 m and the aluminium plates with dimensions $0.625\ \text{m} \times 0.625\ \text{m} \times 0.0008\ \text{m}$ were clamped to the end flange of the tube in an attempt to achieve fixed boundary conditions (Figure 2b-c). The plates had an exposed area of $0.3\ \text{m} \times 0.3\ \text{m}$ (equal to the internal cross-section of the tube).

Table 1. Experimental program and initial conditions.

Test	Pressure driver [kPa]	Ambient pressure [kPa]	Ambient temperature [$^\circ C$]
R05	661.8	100.3	20.5
R7.5	866.4	99.8	22.6
R10	1200.8	100.3	20.8
A05	660.9	100.9	22.3
A7.5	882.2	100.9	22.3
A10	1190.7	100.9	22.1

Piezoelectric pressure sensors (Kistler 603B) were used to measure the pressure 34.5 cm (Sensor 1) and 24.5 cm (Sensor 2) upstream the test specimen (Figure 2a). The pressure sensors were flush mounted in the tube wall, automatically triggered when the shock wave arrived at Sensor 1 and operated with a sampling frequency of 500 kHz. Moreover, the massive plate was equipped with 12 pressure sensors along the vertical, horizontal and diagonal to measure the pressure distribution on a rigid boundary.

To establish a basis for comparison of the structural response in the numerical simulations, the aluminium plates were spray-painted with a speckle pattern (Figure 2c) and three-dimensional digital image correlation (3D-DIC) analyses were used to measure the transient displacement field. The choice of speckle pattern was based on minimizing the effect of aliasing in the DIC calculations [4] and the stereovision setup of the two high-speed cameras (Phantom v1610) is illustrated in Figure 2a. The 3D-DIC was performed using an in-house DIC code (eCorr) comparing the greyscale-value field of the speckle pattern for an image in the deformed (current) configuration to that at the undeformed (reference) configuration. The pressure measurements were synchronized with the high-speed cameras operating at a recording rate of 24 kHz.

The pressure measurements on the massive steel plate were already reported in Ref. [4], while the dynamic response in terms of mid-point deflection histories of the aluminium plates will be presented and compared to the numerical simulations in Section 3.2.

3. Numerical simulations

3.1. Material model

The material was modelled using the *VPJC* material model in EPX [3], which allows for finite strains and rotations, high strain rates, ductile failure and temperature softening. The plasticity is governed by the von Mises yield criterion, the associated flow rule and a modified Johnson-Cook relation for the flow stress. This results in the following dynamic yield function governing the material behaviour [2]

$$f_d(\boldsymbol{\sigma}, p, \dot{p}, T) = \sigma_{eq}(\boldsymbol{\sigma}) - \sigma_y(p,T)\left[1+\frac{\dot{p}}{\dot{p}_0}\right]^c = \sqrt{\frac{3}{2}\boldsymbol{\sigma}':\boldsymbol{\sigma}'} - \left[\sigma_0 + \sum_{i=1}^{2} Q_i(1-\exp(-C_i p))\right]\left[1+\frac{\dot{p}}{\dot{p}_0}\right]^c\left[1-T^{*m}\right] \quad (1)$$

where σ_{eq} is the equivalent von Mises stress, σ_y is the flow stress, p is the equivalent plastic strain, $\dot{p}$ is the equivalent plastic strain rate, $\dot{p}_0$ is a user-defined reference strain rate, σ_0 represents the initial yield stress, (Q_i, C_i, c, m) are material constants and $\boldsymbol{\sigma}'$ is the deviatoric part of the Cauchy stress tensor. The homologous temperature is defined as $T^* = (T - T_r)/(T_m - T_r)$, where T is the absolute temperature, T_r is the ambient temperature and T_m is the melting temperature of the material. Since the structural response from blast events has a very short duration in time, the temperature evolution was modelled assuming adiabatic conditions and calculated based on the plastic dissipation [2]. Thus, Eq. (1) allows for viscoplasticity when $f_d = 0$, while $f_d < 0$ means elastic behaviour.

Ductile failure was also included in the material model by using the Cockcroft-Latham (CL) failure criterion [5] which is an energy-based criterion using the "plastic work" per unit volume to predict failure in the material. The criterion was in this study considered as uncoupled from the constitutive relation and the damage parameter D was expressed as

$$D = \frac{W}{W_c} = \frac{1}{W_c}\int_0^p \langle \sigma_1 \rangle \, dp \,, \qquad \langle \sigma_1 \rangle = \max(\sigma_1, 0) \quad (2)$$

where W_c is the failure parameter found by integrating the major principal stress σ_1 in a uniaxial tension test over the entire equivalent plastic strain path until the plastic strain at failure p_f. Failure occurs when D reaches the critical value $D_c = 1$.

The material parameters were found following exactly the same procedure as in Ref. [1]. That is, the quasi-static parameters (σ_0, Q_i, C_i) were obtained by inverse modelling using a FE model of a representative test in the rolling direction in Section 2.1, while the remaining parameters and physical constants were taken from Ref. [2]. Figure 1a compares the nominal stress-strain curves from the material tests and the FE simulation in EPX with the optimized material parameters, while Figure 1b compares the equivalent stress-plastic strain curve until necking from the representative test to the first term in the expression for the flow stress in Eq. (1). The optimized material parameters are given in Table 2. It is observed that the identified material parameters are able to describe the quasi-static response of the material very well for the tensile tests in the rolling direction.

Table 2. Material parameters and physical constants for the EN AW 1050-H14 aluminium alloy.

σ_0 [MPa]	Q_1 [MPa]	C_1 [-]	Q_2 [MPa]	C_2 [-]	c [-]	m [-]	$\dot{p}_0$ [s^{-1}]	W_c [MPa]	T_r [K]	T_m [K]
80	31.2	1090.0	12.2	20.4	0.014	1.0	5×10^{-4}	60.0	293	893

The CL parameter W_c in Eq. (2) was determined based on the FE simulation by inspecting the element exposed to the largest "plastic work" W. It is emphasized that the W_c parameter found from this approach is mesh-size dependent. This is due to the fact that the element of interest is always located inside the neck and the mesh size will influence the representation of the necking. Only the tension test in the rolling direction of the plate was used in the identification, although the flow stress was higher and the failure strain was somewhat lower in the 45° and 90° directions (see Figure 1a). This implies a spread in W_c between material directions, which (at least to some extent) may affect the numerical results. However, modelling of anisotropy is beyond the scope of this study. The point

used to extract W_c from the FE simulation is indicated by a red dot in Figure 1a, and the value is given in Table 2. The W_c parameter was determined at the same force level as failure occurred in the test under consideration.

3.2. Uncoupled approach

Figure 3 illustrates the numerical model in the uncoupled approach, where the symmetry of the problem was utilized by modelling only one quarter of the clamping assembly using symmetric boundary conditions (Figure 3a). Figure 3b illustrates the full view of the experimental setup obtained by mirroring the quarter model across symmetry planes. The full view of the clamping assembly is only used for visualization purposes. A mesh sensitivity study showed that a mesh size of 10 mm in the plate is adequate to predict the global deformation observed in the experiments. However, the plate was modelled using a Lagrangian discretization with an element size of approximately 6 mm as the base mesh and 4-node Reissner-Mindlin shells (*Q4GS*) with 6 dofs per node and 20 integration points (5 through the thickness). The fine base mesh was chosen in view of the findings regarding AMR and element erosion in Ref. [6].

The material behaviour of the plate was governed by the *VPJC* model with material and physical constants from Table 2. Failure was modelled using element erosion and was initiated when all the integration points in the respective element reached the critical value of unity for the damage parameter in Eq. (2). In an attempt to predict the crack propagation observed in the experiments, it was used AMR driven by the damage parameter D. That is, the mesh refinement occurs at user-defined levels of the damage parameter and at successive levels of refinement. The shells are then refined by splitting each element into four smaller elements using the technique of Ref. [7]. The mesh refinement strategy is also shown in [6] for the quadrilateral shell elements used in this study. It is emphasized that for this approach to predict localization of damage, the mesh should be sufficiently refined relatively long before the element is eroded [6]. This will also reduce the mesh size dependence on the W_c parameter, overcome the challenges related to the spatial discretization in the FE method, and avoid artificial loss of mass when eroding large elements. This study used up to three successive refinements within the range of $0.01 \le D \le 0.20$, resulting in a minimum element size of 0.75 mm when $D > 0.20$.

The bolts and clamping frames were represented by 8-node brick elements (*CUB8*) with 8 integration points and the *VPJC* model with a high elastic limit to ensure elastic behaviour using the physical constants for steel in Ref. [2]. Each bolt was pre-stressed to an initial torque ($M_t = 200$ Nm) in the tests, resulting in a clamping pressure between the frames and the plate. This was accounted for by modelling the lower clamping frame and bolts as one initially stress free component, while an external pressure was applied at the contact area between the bolt head and upper clamping frame (see Figure 3). The contact pressure was determined using the approach suggested in Ref. [2], resulting in a contact pressure of 44 MPa applied throughout the simulation.

The contact between the plate, clamping frames and the bolts was modelled using hierarchic pinballs based on a

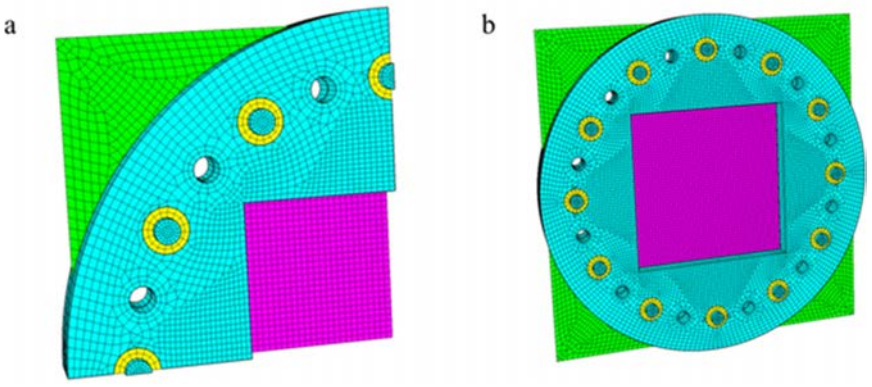

Figure 3. Numerical model in the uncoupled approach: (a) the quarter model and (b) the complete assembly after mirroring across the symmetry planes. The lower clamping frame and the blots are modelled as one component (in cyan), the plate is modelled using shell elements (in green) where the pressure is applied on the exposed area (in magenta), and the upper clamping frame (also in cyan) is applied a pressure in the contact area (in yellow) between the frame and the bolts.

direct penalty method. Three different bodies were identified for the pinballs definition, i.e., the lower clamping frame merged with the bolts, the plate and the upper clamping frame. The thickness of the plate was accounted for by applying a gap of 0.4 mm (i.e., half of the plate thickness) between the plate and the clamping frames to avoid initial penetrations in the contact surfaces. The friction coefficient between the clamping frames and the plate was set to 0.5 (both static and dynamic coefficients), a typical value from the literature for an aluminium on steel interface. Further details of this contact method can be found in Ref. [6].

The loading was applied using the pressure histories from the massive plate tests in Section 2.2 with similar blast intensities to the tests with thin aluminium plates. That is, the loading measured at the massive plate in test RY was assumed to be valid also for test AY. The uncoupled approach makes the inherent assumption that the pressure is unaltered by the plate deformation, which is a simplification of the real behaviour. The modified Friedlander equation is typically used to represent the pressure-time history when the parameters governing the positive phase of a blast load are known [2][4], i.e.,

$$p_r(t) = p_1 + p_{\mathrm{r,max}}\left(1-\frac{t-t_a}{t_{d+}}\right)\exp\left(\frac{-b(t-t_a)}{t_{d+}}\right), \qquad t_a < t < t_a + t_{d+} \tag{3}$$

where $p_{\mathrm{r,max}}$ is the peak reflected overpressure, p_1 is the ambient pressure, t_a is the time of arrival of the blast wave at the target, $t_{\mathrm{d+}}$ is the duration of the positive phase and b is the exponential decay coefficient. The positive specific impulse $i_{\mathrm{r+}}$ has an analytical solution given by

$$i_{r+} = \int_{t_a}^{t_a+t_{d+}} p_r(t)dt = \frac{p_{\mathrm{r,max}}t_{d+}}{b^2}\left[b-1+\exp(-b)\right] \tag{4}$$

The blast parameters $p_{\mathrm{r,max}}$, t_{d+} and i_{r+} may then be used to iteratively find the exponential decay coefficient b in Eq. (4). This enables the corresponding Friedlander curve to be expressed by Eq. (3). The pressure measurements from the RY tests were therefore idealized by curve-fitting to the Friedlander equation using Eqs. (3)-(4) and imposed as a uniformly distributed pressure on the exposed area of the aluminium plates. These loading parameters are given in Ref. [4], but also repeated in Table 3 for the completeness of this study.

Table 3. Friedlander parameters curve-fitted to the pressure measurements in the massive plate tests.

Test	$p_{\mathrm{r,max}}$ [kPa]	$t_{\mathrm{d+}}$ [ms]	$i_{\mathrm{r+}}$ [kPa ms]	b [-]
R05	166.3	20.9	1316.8	0.900
R7.5	196.3	23.6	1675.6	1.011
R10	276.7	27.3	2587.2	1.237

Finally, the influence of the boundary conditions was investigated by comparing the dynamic response in the clamped assembly to that in a simplified model. The simplified model contained only the exposed area of the plate (magenta in Figure 3) where all the nodes located along the perimeter were fully fixed against translation in all directions.

The numerical results in terms of mid-point deflections are compared to the experimental data in Figure 4. No deformation histories were recorded in test A10 due to a synchronization error with the high-speed cameras. The displacement histories reported in Figure 4 are therefore limited to tests A05 and A7.5. All tests experienced inelastic deformations with a permanent deflection in the same direction as the incident blast wave, where it was observed an increased mid-point deflection at increasing blast intensities. In general, the mid-point deflections were overestimated in both the clamped assembly and the simplified model when using the uncoupled approach. As expected, the deflections in the simplified model were slightly less than those in the clamped assembly. It is important to emphasize that although the simplified model is closer to the experimental data for the uncoupled approach in Figure 4, this model does not necessarily provide better predictions than the clamped assembly. This is due to the fact that the loading in the uncoupled approach neglects FSI effects and is therefore conservative.

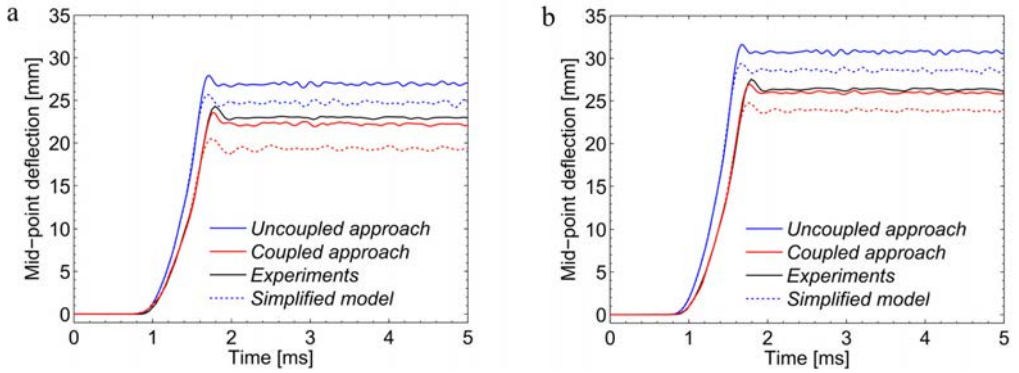

Figure 4. Mid-point deflections in the numerical simulations of the blast-loaded aluminium plates: (a) test A05 and (b) test A7.5. The uncoupled and coupled approaches are compared to investigate the influence of FSI effects during the dynamic response, while the simplified models are included to indicate the effect of the boundary conditions.

Despite some synchronization problems in the camera recordings during the A10 test, this experiment resulted in complete failure along the boundary and the images therefore serve as a qualitative basis for comparison of the dynamic failure in the simulation of test A10 (Figure 5). It is observed that the numerical model does not predict exactly the same failure pattern as in the experiment. The experimental observations showed crack initiation and tearing along the right vertical (Figure 5a) before the cracks propagated along the upper and lower horizontals (Figure 5b) and the entire plate eventually rotates about the left vertical. This was not the case in the simulations where it was, as expected, observed a symmetric failure pattern with crack growth initiation from the centre of the boundary propagating towards the corners of the plate (Figure 5b). A possible explanation for this deviation is the slight anisotropy of the material, as shown in Figure 1a. However, the simulation of the A10 test indicates that the

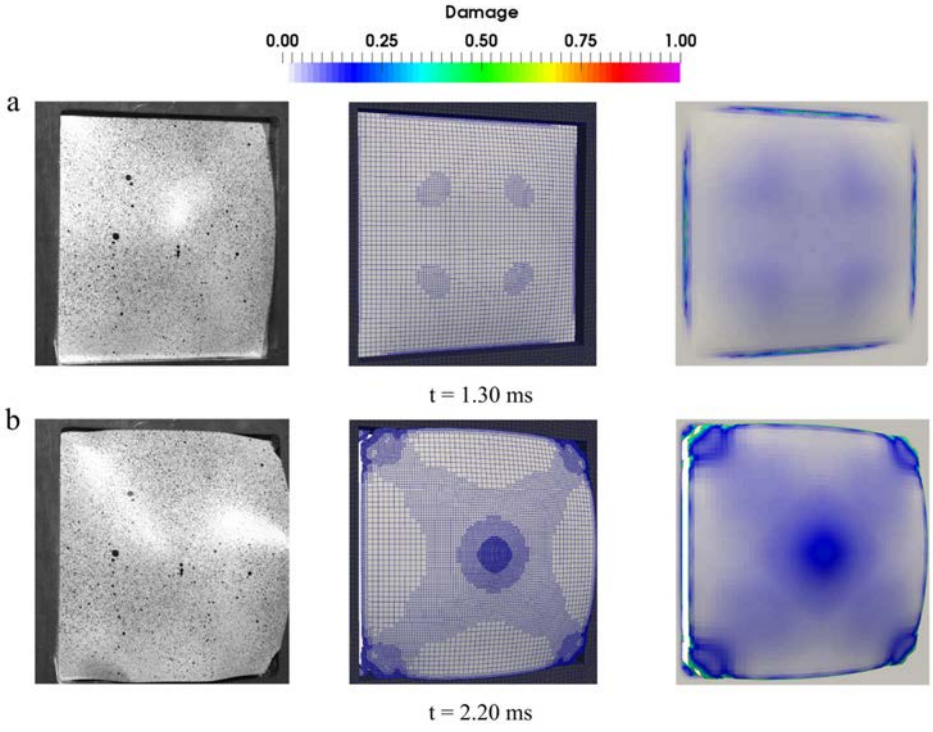

Figure 5. Comparison of crack growth in test A10 and corresponding uncoupled simulation. The deformed configurations are shown with (middle) and without (right) mesh lines, and compared to the experiment (left). Fringe colors represent the damage parameter in Eq. (2).

relatively simple failure criterion in combination with element erosion and AMR is capable of predicting failure at more or less the same point in time.

The influence of damage-based AMR in predicting ductile failure in the plates was investigated by comparing the AMR simulations with the results from numerical models using uniform mesh sizes of 0.75 mm and 6.0 mm in the plate. It was found a significant effect of AMR both in terms of the predicted crack pattern and also of the CPU cost. A uniform mesh of 6 mm did not predict any failure in the A10 test since larger elements diffuse the localization and failure process, while a uniform mesh of 0.75 mm predicted the same failure pattern as that with AMR but at a significant increase in CPU cost (approximately 5 times the cost as with AMR).

3.3. Coupled approach

To investigate the influence of FSI effects on the response of the aluminium plates, it was established a fully coupled FSI model of the entire experimental setup in Figure 2a. The uncoupled approach then serves as a basis for comparison of the coupled simulations to identify potential FSI effects during the dynamic response.

The pressure measurements on the massive plate tests showed that the blast wave may be considered as planar over the cross-section of the tube (see also Ref. [4]). The fluid sub-domain in the fully coupled simulations was therefore modelled as 1D until 0.6 m upstream the test specimen. That is, the fluid sub-domain was partly meshed by 1D finite volumes (*TUVF*) and partly by 3D finite volumes (*CUVF*). This is illustrated in Figure 6 where it was used an initial mesh size of 0.01 m in the entire 1D-domain and in the vicinity of the plate, whereas the cell size in the tank was increased up to 0.08 m towards the internal walls. This resulted in 1587 *TUVF*s and 105,855 *CUVF*s in the fluid sub-domain. The conservation laws of mass, momentum and energy are then expressed in a spatial framework. This is known as the Eulerian formulation and considers the computational mesh fixed while the fluid (particles) moves relative to these grid points. While a FE discretization is typically used for structural applications (as in Section 3.2), the most suitable discretization within computational fluid dynamics is based on finite volume (FV) formulations. FVs are another way of expressing the conservation laws in which the governing equations for the computational cells are formulated and solved in integral form. This method is conservative since the formulation ensures that the flux entering a given volume is identical to that leaving the adjacent volume. Thus, the FV method require less smoothness of the solution compared to the FE method which is favourable in nearly discontinuous solutions such as blast waves (see e.g. Ref. [8]). The fully coupled simulations therefore use the FE discretization presented in Section 3.2 for the aluminium plate and clamping frames, and FVs in the fluid sub-domain. Then, the numerical fluxes between adjacent FVs were calculated using the approximate Harten-Lax-van-Leer-Contact (HLLC) Riemann solver [3], where stability in the convection phase of the explicit solution in time

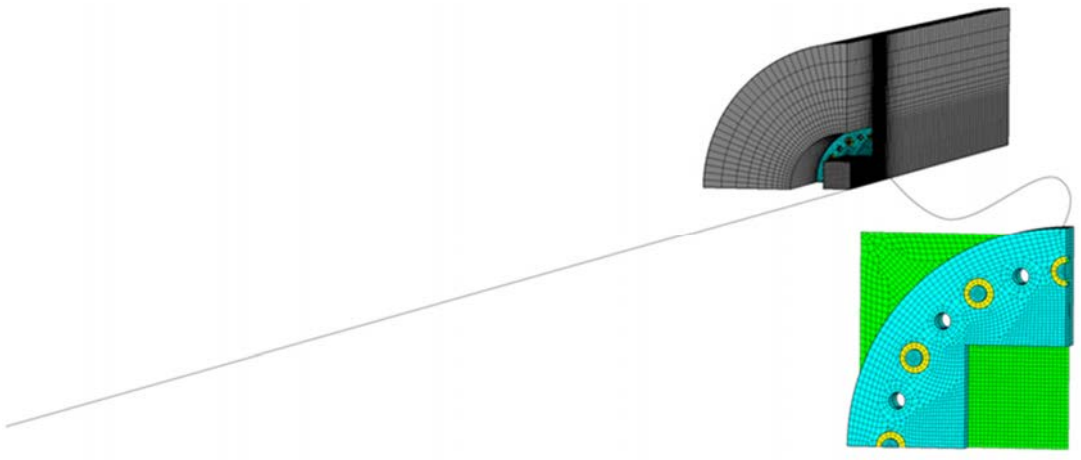

Figure 6. Computational model for the fully coupled FSI simulations. The plate in Figure 3a is embedded into the fluid sub-domain (grey color), where most of the driver and driven sections are modelled as 1D finite volumes (shown as a thin line).

was ensured by using a Courant-Friedrichs-Lewy coefficient of 0.4. An embedded FSI technique (*FLSW*) [3][9] was used for the coupling at the fluid-structure (F-S) interface and FSI-driven AMR was also activated in the fluid sub-domain to obtain a sufficiently refined fluid mesh at the F-S interface. The air was modelled using the equation of state for the ideal gas material (*GAZP*) [3] and the initial conditions for each simulation were taken from the aluminium plate tests in Table 1. Friction and heat exchange against the interior walls of the tube were accounted for by specifying the average roughness (0.4 micrometers) in the *PARO* directive in EPX [3].

The mid-point deflections from the fully coupled simulations are compared to the uncoupled approach and experimental data in Figure 4 in an attempt to identify FSI effects. It is observed that the mid-point deflections are reduced by approximately 15 % when considering FSI, and that the fully coupled simulations with the clamped assembly model of the plate (red solid lines in Figure 4) result in an excellent agreement with the experimental observations. This indicates that fully coupled simulations are necessary to obtain a quantitatively correct agreement with the experimental data in terms of the dynamic response. Comparing the CPU time at 5 ms for the uncoupled and coupled approaches in Figure 4, the increase in CPU cost in the fully coupled simulations was estimated to be in the order of 50-90 %. It should be noted that the failure patterns in Figure 5 were also observed in the coupled simulations for the A10 test.

4. Concluding remarks

The fully coupled simulations were in excellent agreement with the experimental data, whereas the uncoupled approach over-predicted the dynamic response by approximately 15 %. This illustrates the importance of an accurate loading description and of accounting for FSI effects when predicting the dynamic response of blast-loaded flexible plates. The numerical simulations also indicated that the dynamic failure could be predicted by element erosion and a relatively simple energy-based criterion. The use of damage-based AMR was promising in terms of predicting ductile failure in blast-loaded plates without too much loss of mass and at a reasonable CPU cost. This may be interesting in blast-resistant design of plated structures since these are typically made with geometries that closely resemble shell structures, i.e., one of the dimensions (typically the thickness) is significantly smaller than the others. Such structures often require a fine mesh size to represent localization of damage and crack growth. However, further investigations are needed to better understand and ensure an appropriate use of damage-based AMR in engineering applications. These improvements are left for future work.

Acknowledgements

The present work has been carried out with financial support from SFI-SIMLab and SFI-CASA at the Norwegian University of Science and Technology (NTNU).

References

[1] V. Aune, E. Fagerholt, K. O. Hauge, M. Langseth, T. Børvik, Experimental study on the response of thin aluminium and steel plates subjected to airblast loading, International Journal of Impact Engineering 90 (2016) 106–121.

[2] V. Aune, G. Valsamos, F. Casadei, M. Larcher, M. Langseth, T. Børvik, Numerical study on the structural response of blast-loaded thin aluminium and steel plates, International Journal of Impact Engineering 99 (2017) 131–144.

[3] EUROPLEXUS user's manual, Joint Research Centre, http://europlexus.jrc.ec.europa.eu/ [cited 13.03.2017].

[4] V. Aune, E. Fagerholt, M. Langseth, T. Børvik, A shock tube facility to generate blast loading on structures, International Journal of Protective Structures 7 (2016) 340–366.

[5] M. G. Cockcroft, D. J. Latham, Ductility and the workability of metals, Journal of the Institute of Metals, 96 (1968) 33-39

[6] V. Aune, G. Valsamos, F. Casadei, M. Langseth, T. Børvik, On the dynamic response of blast-loaded steel plates with and without pre-formed holes, International Journal of Impact Engineering (2017). DOI: 10.1016/j.ijimpeng.2017.04.001. Article in Press.

[7] F. Casadei, P. Diez, F. Verdugo, An algorithm for mesh refinement and un-refinement in fast transient dynamics, International Journal of Computational Methods 10 (2013) 1–31.

[8] M. Larcher, F. Casadei, Explosions in complex geometries – a comparison of several approaches, International Journal of Protective Structures 1 (2010) 169–196.

[9] F. Casadei, M. Larcher, N. Leconte, Strong and weak forms of a fully non-conforming FSI algorithm in fast transient dynamics for blast loading of structures, Proceedings of the COMPDYN 2011 Conference, Corfu, Greece, May 25-28, 2011.